

# Joint PP and PS AVA seismic inversion using exact Zoeppritz equations

Jun Lu<sup>1</sup>, Zhen Yang<sup>1</sup>, Yun Wang<sup>2</sup>, and Ying Shi<sup>1</sup>

## ABSTRACT

The Zoeppritz equations describe the relationship between seismic properties that are useful for the interpretation of lithology and fluid properties. Various approximations to the Zoeppritz equations are often used in linear amplitude variation with offset and amplitude variation with angle inversions, assuming low-contrast boundaries. These approximations restrict the inversion method to not-too-large-angle cases and reduce the inversion accuracy. Therefore, it is necessary to develop joint PP and PS prestack inversion methods using the exact Zoeppritz equations. We have developed a method for nonlinear joint prestack inversion using the exact Zoeppritz equations. We established an objective function to combine PP and PS information based on a

least-squares approach, and we used the Taylor expansion method to derive a model updating formula for the inversion. We also used a mean shift method to improve the accuracy of inversion results. We validated our inversion using synthetic and field seismic data. The model for calculating synthetic data contained high-contrast interfaces to match the reservoir layers, which included, for example, coal seams and unconsolidated sandstone. The outputs of the inversion were the elastic parameters (P- and S-wave velocities, as well as density), rather than the changes in elastic parameters. We found that the nonlinear joint prestack inversion achieved more accurate results than the linear joint prestack inversion, regardless of incidence angle size. Furthermore, if the prestack data were of high enough quality, it was possible to identify thin layers from the inversion result.

## INTRODUCTION

The technique of amplitude variation with offset (AVO), or amplitude variation with incidence angle (AVA), has been used to predict lithology and fluid properties for decades (Ostrander, 1982; 1984; Sun et al., 2008). The Zoeppritz equations describe the relationship between reflection and transmission coefficients for a given incidence angle, and elastic media properties (P- and S-wave velocities, as well as density). Because the Zoeppritz equations are nonlinear functions with respect to these properties, many approximations have been made to linearize them to simplify calculations. These approximations have played a key role in the estimation of elastic parameters by AVO/AVA inversions.

P-wave AVO/AVA methods have been developed over decades and remarkable advances have been achieved. Since Ostrander (1982) proposes an AVO method to extract lithology and pore-fluid

information from prestack seismic amplitudes, AVO has been used with varying rates of success (Larsen, 1999). Shuey (1985) develops a gradient-intercept method that estimates zero-offset reflectivity and changes in Poisson's ratio. Smith and Gidlow (1987) estimate rock properties by a weighted stacking method using time- and offset-variant weights to PP data samples before stacking. Roberts et al. (2002) use an AVO method to enhance the reservoir characterization based on the long-offset seismic data. However, a few years of experience in P-mode AVO observation leads to results that are sometimes too ambiguous to interpret (Jin, 1999).

Compared with P-wave approaches alone, joint AVO inversion of PP and PS data can provide better estimates of elastic parameters (Kurt, 2007); however, most AVO studies use two-parameter inversion methods because three-parameter inversions are often plagued by numerical instability (Ursenbach and Stewart, 2008). Stewart (1990) extends the weighted stacking method to invert PP- and

Manuscript received by the Editor 15 October 2014; revised manuscript received 23 May 2015; published online 29 July 2015.

<sup>1</sup>China University of Geosciences, Key Laboratory of Marine Reservoir Evolution and Hydrocarbon Accumulation Mechanism, Ministry of Education, Beijing, China. E-mail: lujun615@163.com; zhendexiangzi@yahoo.com; quartzsy@163.com.

<sup>2</sup>Chinese Academy of Sciences, Institute of Geochemistry, Guiyang, China. E-mail: yunwang@mail.iggcas.ac.cn.

© The Authors. Published by the Society of Exploration Geophysicists. All article content, except where otherwise noted (including republished material), is licensed under a Creative Commons Attribution 4.0 Unported License (CC BY). See <http://creativecommons.org/licenses/by/4.0/>. Distribution or reproduction of this work in whole or in part commercially or noncommercially requires full attribution of the original publication, including its digital object identifier (DOI).

PS-waves jointly for rock property estimations. Fatti et al. (1994) improve the weighted stacking method to directly estimate fractional P and S impedance, but their method requires the angle of incidence less than  $35^\circ$  and P- to S-wave velocity ratios between 1.5 and 2.0. Xu and Bancroft (1997) express the P-P and P-S reflection coefficient equations with the elastic parameters ( $\lambda$  and  $\mu$ , or  $\kappa$  and  $\mu$ ) and extract these parameters directly without conversion from velocity. Larsen (1999) presents a method to invert PP and PS AVO gathers simultaneously to estimate P and S impedance. Ursenbach and Stewart (2008) derive inversion error expressions for various two-parameter inversion methods, and obtain flexible conversion formulas that can convert the results of any two-parameter method to those of any other two-parameter method. However, two-parameter methods lose important density information, an AVO attribute that is useful for inferring fluid saturation (Downton, 2005).

For this reason, a significant amount of work has been done on elastic three-parameter estimations. Jin (1999) presents a real data example of a joint P- and S-wave AVO analysis that estimates elastic parameters for reservoir characterization, and proposes that S-wave data gave the opportunity to estimate S-wave velocity and density variations. Jin et al. (2000) use singular-value decomposition (SVD) to stabilize the linearized PS system of equations, and they obtain good results for synthetic and field data. Buland and Omre (2003) develop a new linearized AVO inversion method using Bayesian techniques to obtain P- and S-wave velocities, as well as density distributions. Mahmoudian and Margrave (2004) formulate the joint AVO inversion using SVD methods to obtain P- and S-impedance contrasts, as well as density contrast. Three-parameter inversion methods are also investigated by Downton and Lines (2004), Mahmoudian (2006), and Veire and Landrø (2006), but all these studies solve approximations of the Zoeppritz equations. The underlying assumption of these approximations is that the incidence angle is not too large and the contrast in elastic parameters is weak (Aki and Richards, 1980; Zhi et al., 2013); however, these approximations affect the accuracy of calculations, and they are particularly unsuitable in the case of a strong contrast between layers, such as that between a coal seam and unconsolidated sandstone. Therefore, a joint AVO/AVA inversion method using exact Zoeppritz equations would represent a more robust method of estimating elastic parameters using multicomponent seismic data (Zhi et al., 2013).

Some attempts at solving the exact Zoeppritz equations have been made. For example, Tigrek et al. (2005) develop a method to relate the offset-dependent seismic reflections to the local stress distributions, and obtain accurate result by joint AVA analysis based on the full-Zoeppritz equations. Wang et al. (2011) estimate model parameters with the exact Zoeppritz equations using a generalized linear inversion. Zhu and McMechan (2012) propose a new algorithm using the exact Zoeppritz equations to obtain four independent parameters (a density ratio and three velocity ratios) for PP reflections. Zhi et al. (2013) rewrite the exact Zoeppritz equations as a function of four independent parameters to invert PP- and PS-waves jointly; however, these inversion results are elastic parameter contrasts, not the elastic properties themselves.

In this paper, we present a method of joint AVA inversion using the exact Zoeppritz equations for PP and PS seismic data. The inverted parameters are P- and S-wave velocities, as well as density. Using a least-squares approach, we establish a joint objective func-

tion that is used to judge whether the difference between simulated and observed records is small enough to end the inversion. To apply the method to field data, some preprocessing is needed, such as true-amplitude processing of the PP and PS data and compression of the PS AVA data set to the PP travelttime domain. The performance of the proposed method is determined by comparison with the synthetic and field seismic data. We also compare the results of the linear and nonlinear joint AVA inversion methods.

## METHODOLOGY

For a welded solid-solid interface between two homogeneous isotropic elastic half-spaces, the P- and S-wave velocities, as well as the density of the upper half-space are denoted by  $\alpha_1$ ,  $\beta_1$ , and  $\rho_1$ , respectively; and in the lower half-space by  $\alpha_2$ ,  $\beta_2$ , and  $\rho_2$ . When a plane P-wave propagates across the interface with a nonzero incidence angle, reflecting and transmitting P- and S-waves are generated, and can be described by the Zoeppritz equations. Accurate solutions of the Zoeppritz equations for PP- and PS-wave reflection coefficients were given by Aki and Richards (1980) as

$$R_{PP} = \left[ \left( b \frac{\cos i_1}{\alpha_1} - c \frac{\cos i_2}{\alpha_2} \right) F - \left( a + d \frac{\cos i_1}{\alpha_1} \frac{\cos j_2}{\beta_2} \right) H p^2 \right] / D \quad (1)$$

and

$$R_{PS} = -2 \frac{\cos i_1}{\alpha_1} \left( ab + cd \frac{\cos i_2}{\alpha_2} \frac{\cos j_2}{\beta_2} \right) p \alpha_1 / (\beta_1 D), \quad (2)$$

where

$$\begin{cases} a = \rho_2(1 - 2\beta_2^2 p^2) - \rho_1(1 - 2\beta_1^2 p^2), \\ b = \rho_2(1 - 2\beta_2^2 p^2) + 2\rho_1\beta_1^2 p^2, \\ c = \rho_1(1 - 2\beta_1^2 p^2) + 2\rho_2\beta_2^2 p^2, \\ d = 2(\rho_2\beta_2^2 - \rho_1\beta_1^2) \end{cases} \quad (3)$$

and

$$\begin{cases} E = b \frac{\cos i_1}{\alpha_1} + c \frac{\cos i_2}{\alpha_2}, \\ F = b \frac{\cos j_1}{\beta_1} + c \frac{\cos j_2}{\beta_2}, \\ G = a - d \frac{\cos i_1}{\alpha_1} \frac{\cos j_2}{\beta_2}, \\ H = a - d \frac{\cos i_2}{\alpha_2} \frac{\cos j_1}{\beta_1}, \\ D = EF + GH p^2. \end{cases} \quad (4)$$

Additionally,  $i_1$  and  $i_2$  are the P-wave angles of incidence and transmission across the interface, respectively, and  $j_1$  and  $j_2$  denote the S-wave angles of incidence and transmission, respectively. The value  $p$  is the ray parameter, which is constant for all layers, and  $p = \sin i_1 / \alpha_1 = \sin i_2 / \alpha_2 = \sin j_1 / \beta_1 = \sin j_2 / \beta_2$  (Aki and Richards, 1980).

Our goal is to invert the elastic parameter vector using PP and PS AVA data sets jointly, based on the exact PP- and PS-wave reflection coefficients. According to a least-squares approach, the joint objective function,  $Q$ , for nonlinear inversion is

$$Q(\mathbf{V}) = w \|\mathbf{S}_{PP} - \mathbf{D}_{PP}\|^2 + (1 - w) \|\mathbf{S}_{PS} - \mathbf{D}_{PS}\|^2, \quad (5)$$

where  $\mathbf{V} = (\boldsymbol{\alpha}, \boldsymbol{\beta}, \boldsymbol{\rho})$ , and it denotes the model parameter vector for the target time window. Here,  $\mathbf{D}_{PP}$  and  $\mathbf{D}_{PS}$  are the real PP and PS AVA data sets, respectively. The  $\mathbf{S}_{PP}$  and  $\mathbf{S}_{PS}$  are the synthetic PP and PS AVA data sets for the given model parameter vector  $\mathbf{V}$ . And

$$\begin{cases} \mathbf{S}_{PP} = \mathbf{W}_{PP} * \mathbf{R}_{PP}, \\ \mathbf{S}_{PS} = \mathbf{W}_{PS} * \mathbf{R}_{PS}, \end{cases} \quad (6)$$

where  $\mathbf{W}_{PP}$  and  $\mathbf{W}_{PS}$  denote the PP- and PS-wavelets, respectively, at a given incidence angle. Here,  $\mathbf{R}_{PP}$  and  $\mathbf{R}_{PS}$  are derived from the exact solutions of the Zoeppritz equations shown in equations 1 and 2. In the following model test, we also use Aki and Richards' (1980) approximations to the Zoeppritz equations for  $\mathbf{R}_{PP}$  and  $\mathbf{R}_{PS}$  to compare the results of linear and nonlinear inversions. The weight factor  $w$  ranging from 0 to 1 is used to qualify the two data sets. When the PP data set is of a higher quality than the PS data set,  $w$  is larger than 0.5; if only the PP data are used during the inversion, then  $w$  is set to 1. In the model tests presented here, the quality of the two data sets is assumed to be equal, so  $w$  is set to 0.5.

Given a forward model parameter vector,  $\mathbf{R}_{PP}$  or  $\mathbf{R}_{PS}$  can be expanded into a truncated Taylor series expansion around  $\mathbf{V} = \mathbf{V}_0$ , where  $\mathbf{V}_0$  is the initial parameter vector. This expanded Taylor series has the form

$$\mathbf{R}_{PX}(\mathbf{V}_0 + \Delta\mathbf{V}) = \mathbf{R}_{PX0}(\mathbf{V}_0) + \mathbf{G}(\mathbf{V})\Delta\mathbf{V}. \quad (7)$$

Here, X denotes P or S,  $\Delta\mathbf{V} = (\Delta\boldsymbol{\alpha}, \Delta\boldsymbol{\beta}, \Delta\boldsymbol{\rho})$ , and  $\Delta\boldsymbol{\alpha}$ ,  $\Delta\boldsymbol{\beta}$ , and  $\Delta\boldsymbol{\rho}$  are the desired updates of the current model vector  $\mathbf{V}_0$ . The  $\mathbf{R}_{PX0}$  is the PP or PS reflection coefficient vector at a different incidence angle to that of the initial model. The Jacobian matrix  $\mathbf{G}$  has the form

$$\mathbf{G} = \begin{bmatrix} \frac{\partial \mathbf{R}_1}{\partial \mathbf{V}_1} & \frac{\partial \mathbf{R}_1}{\partial \mathbf{V}_2} & \dots & \frac{\partial \mathbf{R}_1}{\partial \mathbf{V}_n} \\ \frac{\partial \mathbf{R}_2}{\partial \mathbf{V}_1} & \frac{\partial \mathbf{R}_2}{\partial \mathbf{V}_2} & \dots & \frac{\partial \mathbf{R}_2}{\partial \mathbf{V}_n} \\ \vdots & \vdots & \ddots & \vdots \\ \frac{\partial \mathbf{R}_n}{\partial \mathbf{V}_1} & \frac{\partial \mathbf{R}_n}{\partial \mathbf{V}_2} & \dots & \frac{\partial \mathbf{R}_n}{\partial \mathbf{V}_n} \end{bmatrix}, \quad (8)$$

where the subscripts 1 to  $n$  denote different target time sample sequences.

Substituting equations 6 and 7 into equation 5 gives

$$\begin{aligned} Q(\mathbf{V}) = & w \|\mathbf{W}_{PP} * (\mathbf{R}_{PP} + \mathbf{G}_{PP}\Delta\mathbf{V}) - \mathbf{D}_{PP}\|^2 \\ & + (1 - w) \|\mathbf{W}_{PS} * (\mathbf{R}_{PS} + \mathbf{G}_{PS}\Delta\mathbf{V}) - \mathbf{D}_{PS}\|^2. \end{aligned} \quad (9)$$

Using a least-squares approach, we then have

$$\begin{aligned} \frac{\partial Q(\mathbf{V})}{\partial \Delta\mathbf{V}} = & w [(\mathbf{W}_{PP} * \mathbf{R}_{PP} - \mathbf{D}_{PP})^T (\mathbf{W}_{PP} * \mathbf{G}_{PP}) \\ & + (\mathbf{W}_{PP} * \mathbf{G}_{PP}\Delta\mathbf{V})^T (\mathbf{W}_{PP} * \mathbf{G}_{PP})] \\ & + (1 - w) [(\mathbf{W}_{PS} * \mathbf{R}_{PS} - \mathbf{D}_{PS})^T (\mathbf{W}_{PS} * \mathbf{G}_{PS}) \\ & + (\mathbf{W}_{PS} * \mathbf{G}_{PS}\Delta\mathbf{V})^T (\mathbf{W}_{PS} * \mathbf{G}_{PS})] \\ = & 0, \end{aligned} \quad (10)$$

giving

$$\begin{aligned} \Delta\mathbf{V} = & [w\mathbf{H}_{PP}^T\mathbf{H}_{PP} + (1 - w)\mathbf{H}_{PS}^T\mathbf{H}_{PS}]^{-1} \\ & \cdot [w\mathbf{H}_{PP}^T\mathbf{E}_{PP} + (1 - w)\mathbf{H}_{PS}^T\mathbf{E}_{PS}]. \end{aligned} \quad (11)$$

Here,  $\mathbf{H}_{PX} = \mathbf{W}_{PX} * \mathbf{G}_{PX}$  and  $\mathbf{E}_{PX} = \mathbf{D}_{PX} - \mathbf{W}_{PX} * \mathbf{R}_{PX0}$ . The value  $\mathbf{E}_{PX}$  is the residual matrix between the real seismic data and the forward model response for the initial elastic parameters. We use  $\Delta\mathbf{V}$  to update the initial model parameter vector  $\mathbf{V}_0$  iteratively until the joint objective function  $Q$  reaches a minimum. Equation 11 is an unstable solution. Therefore, we use the Levenberg-Marquardt method (Levenberg, 1944; Marquardt, 1963) to solve the singular nonlinear equations, and we modify equation 11 to

$$\begin{aligned} \Delta\mathbf{V} = & [w\mathbf{H}_{PP}^T\mathbf{H}_{PP} + (1 - w)\mathbf{H}_{PS}^T\mathbf{H}_{PS} + \eta\mathbf{I}]^{-1} \\ & \cdot [w\mathbf{H}_{PP}^T\mathbf{E}_{PP} + (1 - w)\mathbf{H}_{PS}^T\mathbf{E}_{PS} + \eta\mathbf{I}], \end{aligned} \quad (12)$$

where  $\eta$  is a Lagrange multiplier and  $\mathbf{I}$  is an identity matrix.

To ensure the inversion accuracy, a mean shift method was applied to constrain the inversion result. After some iterations, we derive an elastic parameter model that is close to the prior model by extrapolating from the well model along horizons. If the ratio between the mean value of the inverse elastic parameters and the prior model parameters is large, then this ratio is used to scale the inverse model to improve its proximity to the prior model. Mean shift can be considered as the low-frequency compensation of the model.

To apply the above method to field PP- and PS-waves, special processing techniques are needed for: (1) P- and S-mode separation from vertical and horizontal components, (2) PS to PP time alignment, and (3) wavelet extraction at different incidence angles.

### P- and S-mode separation from vertical and horizontal components

In multicomponent seismology, multiple field shot records are measured (shown as "mode leakage"), allowing for potential cross-contamination of P-wave energy in the horizontal component and S-wave energy in the vertical component. Suppressing mode leakage by P- and S-wave separation is an important step in prestack multicomponent seismic data processing. For this study, we applied the method introduced by Lu et al. (2012) to separate different wave modes.

### PS to PP time alignment

Owing to the use of a joint objective function during the inversion, the PS time should be aligned with PP time by compressing PS time. To do this, the PS events need to match to the PP events from the same geologic strata with the help of well data and synthetic records. An instantaneous gamma volume  $\gamma_i$  can be derived after accurate horizon matching:

$$\gamma_i = T_{PPi}/T_{PSj}, \quad (13)$$

where  $T_{PPi}$  denotes the PP reflection time for sample  $i$ , and  $T_{PSj}$  denotes the PS reflection time for sample  $j$ . Samples  $i$  and  $j$  are from the same depth. We use  $\gamma_i$  to compress the PS AVA data set to the PP time-domain sample by sample.

**Wavelet extraction at different incidence angles**

The inversion output is the elastic parameter vector, rather than the change in an elastic parameter, so wavelets must be defined. Some prestack processing procedures, such as *Q*-compensation, event stretching, and compression, may lead to the changes of PP- and PS-wavelets at each incidence angle. Wavelets should therefore be extracted from PP and PS data sets separately for the joint inversion, at the total incidence angle. Most other wavelet-extraction methods for PP-waves are suitable for our inversion method. For example, a statistical method of kurtosis maximization by constant-phase rotation developed by Baan (2008) can produce a stationary, constant-phase wavelet (Jonathan and Baan, 2011).

**SYNTHETIC DATA TEST**

To test our method against synthetic data, we used a five-layer 1D model with high-contrast interfaces (shown in Table 1), and synthetic PP and PS AVA data sets within critical angles, as shown in Figure 1. To correlate the PP and PS events, we change the polarities of PS-waves to match those of PP-waves when they are opposite. These data sets are generated with a 1-ms sample rate through convolution of the reflectivity derived from the exact Zoeppritz equation and Ricker wavelets with dominant frequencies of 40 Hz for PP-waves and 30 Hz for PS-waves in PP time, respec-

**Table 1. Theoretical model parameters.**

$\alpha$ (m/s)	$\beta$ (m/s)	$\rho$ (g/cm <sup>3</sup> )	Thickness (m)
2800	933	2.28	100
3200	1600	2.35	100
2000	1333	2.0	3
3300	1650	2.35	80
3400	1700	2.52	390

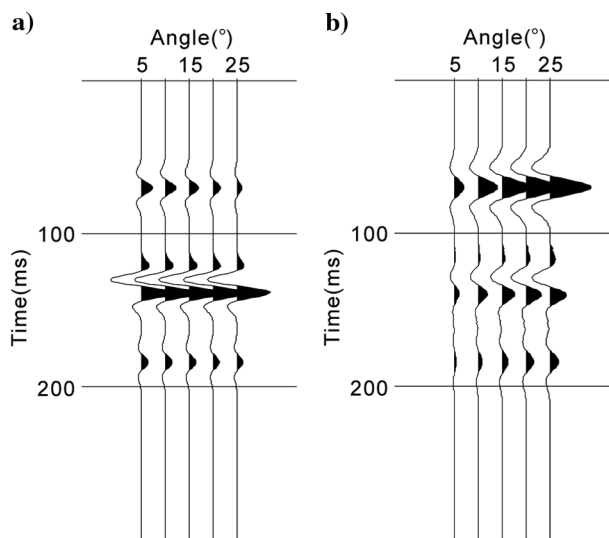


Figure 1. Synthetic (a) PP and (b) PS seismograms in the PP time domain without noise.

tively. Interference, such as noise and multiples, was not taken into account in the forward modeling. Two different inversion models were tested: (1) the nonlinear joint PP and PS AVA inversion based on exact PP and PS reflection coefficients presented above (NJI)

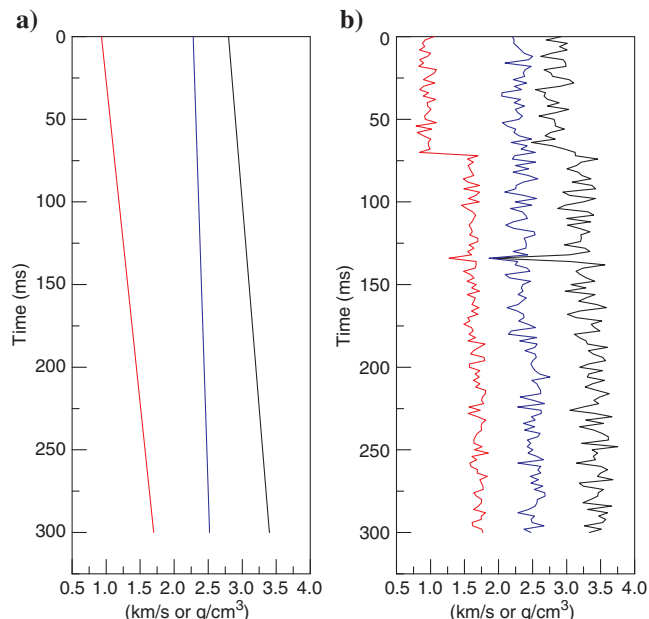


Figure 2. (a) Linear initial model and (b) noise-added initial model generated from the actual model plus 5% random noise. The red curve is the S-wave initial model, the blue curve is the density initial model, and the black curve is the P-wave initial model. These models are used to test the influence of the initial model on the inversion result.

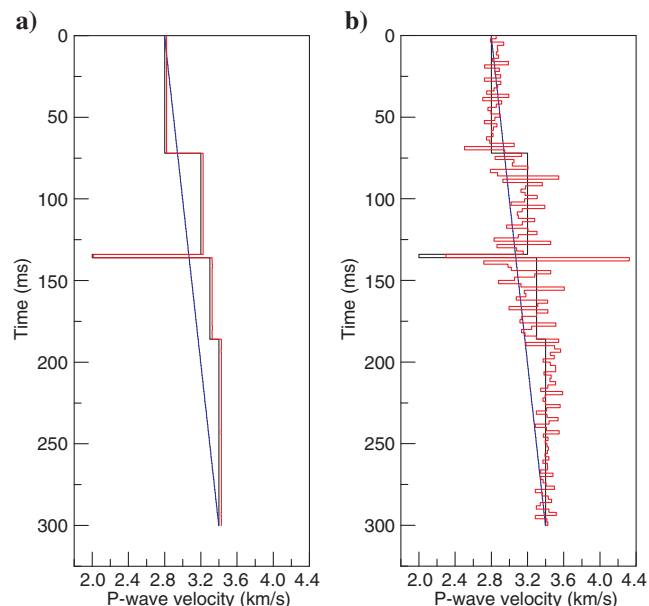


Figure 3. P-wave velocity inversion results inverted by (a) NJI and (b) LJI using the linear initial model. The blue curve is the initial model, the red curve is the inverse result, and the black curve is the true model.

and (2) a linear joint PP and PS AVA inversion based on [Aki and Richards' \(1980\)](#) approximate PP and PS reflection coefficients (LJI). The linear single PP AVA inversion based on [Aki and Richards' \(1980\)](#) approximate PP reflection coefficients (LSI) is also tested. But the results of LSI are closed to that of LJI, so we just

show the results of NJI and LJI for comparison. For joint inversions, the weight factor  $w$  was set to 0.5 (i.e., the two data sets were assumed to have equal quality). For nonlinear and linear inversions, the Jacobian matrix  $G$  was constructed using equation 8, although the nonlinear inversion used the exact Zoeppritz

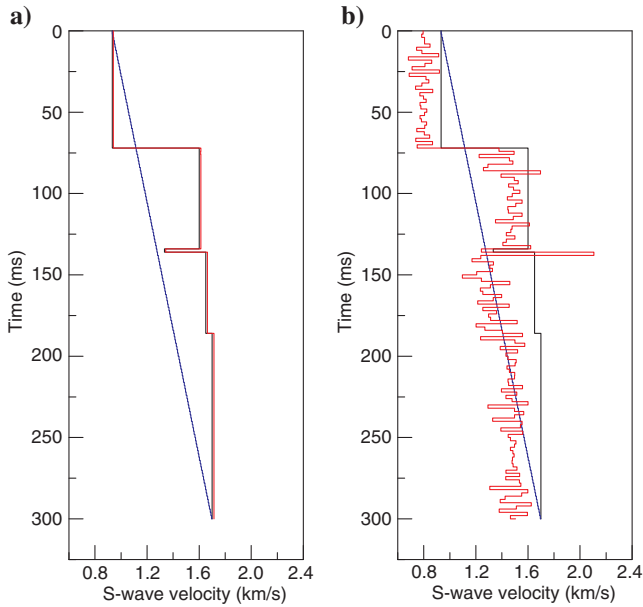


Figure 4. S-wave velocity inversion results inverted by (a) NJI and (b) LJI using the linear initial model. The blue curve is the initial model, the red curve is the inverse result, and the black curve is the true model.

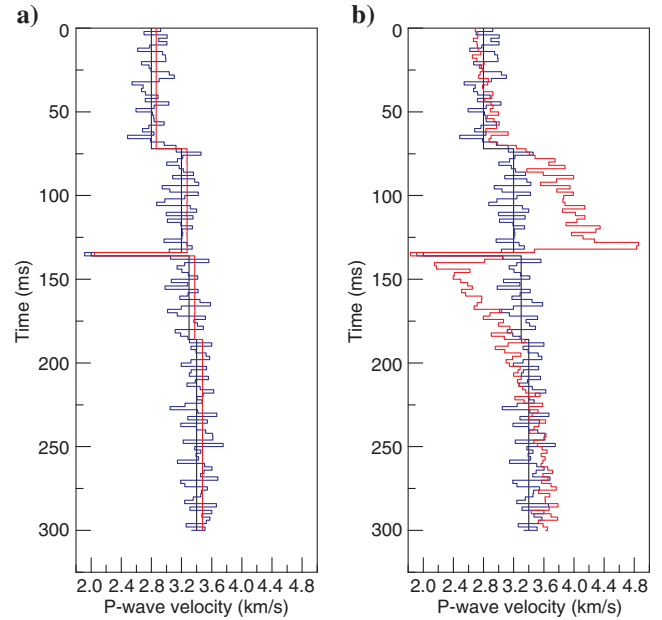


Figure 6. P-wave velocity inversion results inverted by (a) NJI and (b) LJI using the 5% noise-added initial model. The blue curve is the initial model, the red curve is the inverse result, and the black curve is the true model.

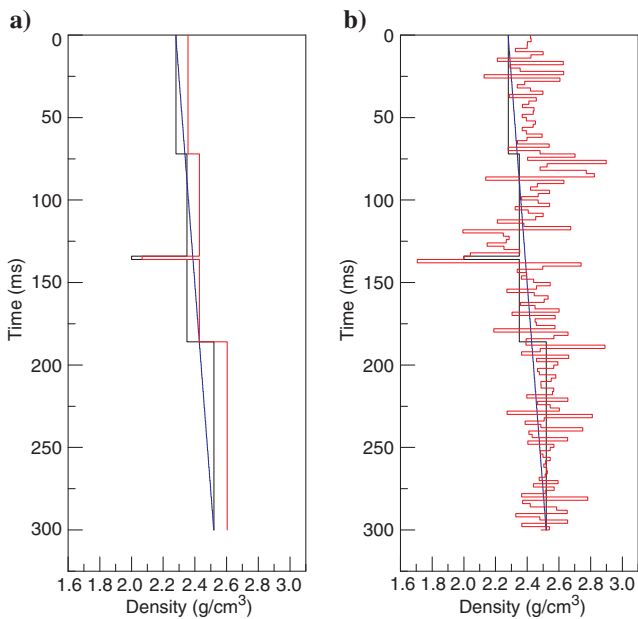


Figure 5. Density inversion results inverted by (a) NJI and (b) LJI using the linear initial model. The blue curve is the initial model, the red curve is the inverse result, and the black curve is the true model.

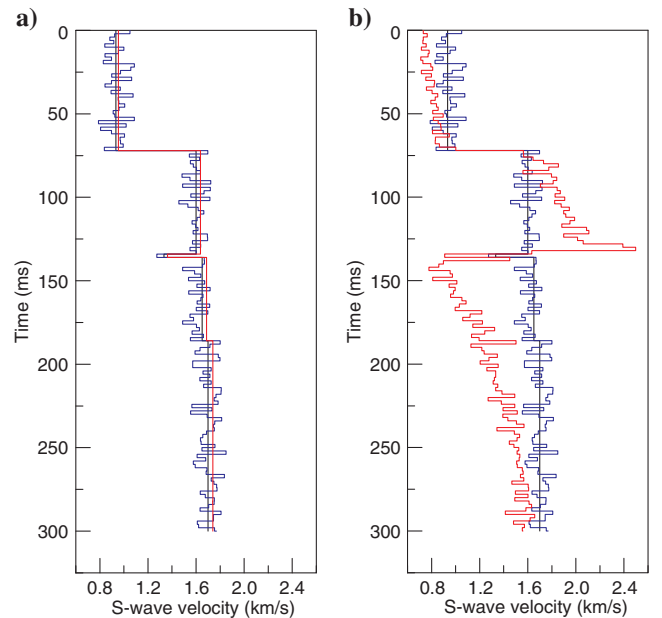


Figure 7. S-wave velocity inversion results inverted by (a) NJI and (b) LJI using the 5% noise-added initial model. The blue curve is the initial model, the red curve is the inverse result, and the black curve is the true model.

solutions, whereas the linear inversion used Aki and Richards' (1980) approximations.

A linear model and a noise-added model (shown in Figure 2) were used to test the sensitivity of our inversion method to the choice of the initial model. The inversion results (without any mean shift corrections) with the linear initial model using the (a) NJI and (b) LJI methods are shown in Figures 3–5 for P- and S-wave velocities, as well as density, respectively. Although the stratigraphic contrast cannot be seen on the plot of the linear initial model (Figure 2a), NJI (Figures 3a, 4a, and 5a) produces a good result, showing a thin layer that exactly conforms to the true model. In contrast, LJI (Figures 3b, 4b, and 5b) produce poor results because

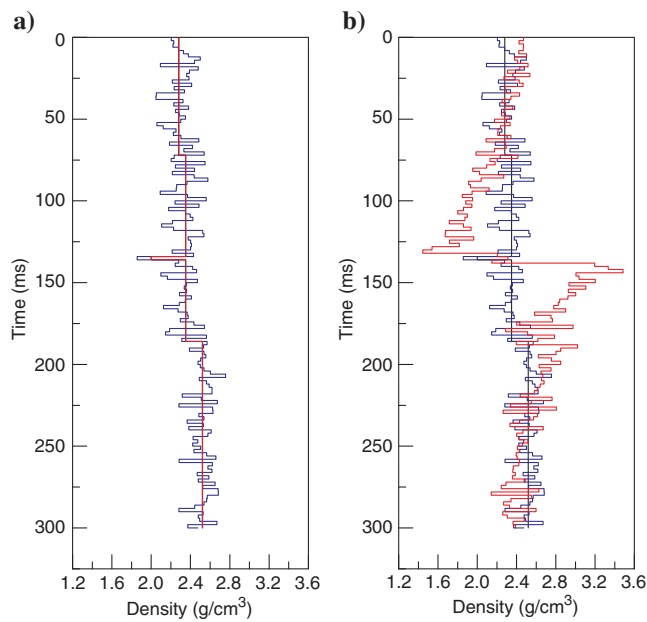
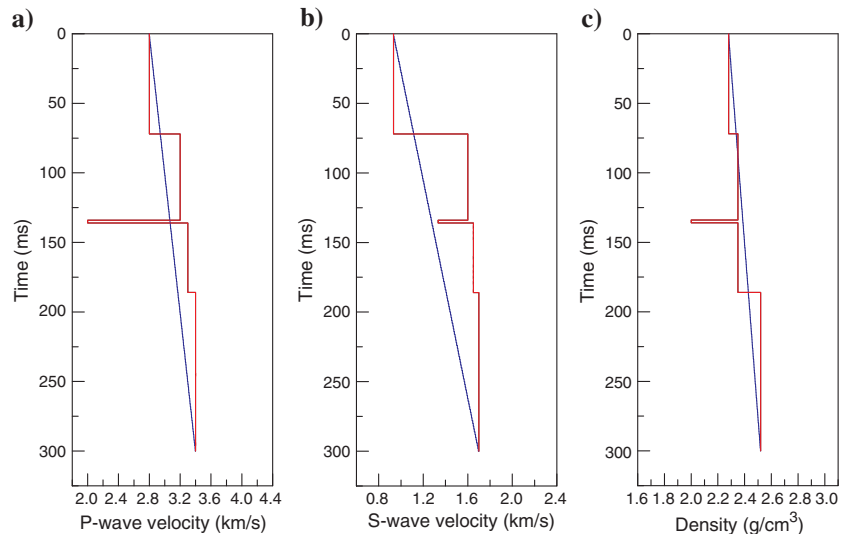


Figure 8. Density inversion results inverted by (a) NJI and (b) LJI using the 5% noise-added initial model. The blue curve is the initial model, the red curve is the inverse result, and the black curve is the true model.

Figure 9. Mean shift in (a) P-wave velocity, (b) S-wave velocity, and (c) density inverted by the NJI method from the linear initial model. The blue curve is the initial model, and the red curve is the inverse result, which is coincident with the true model.



the true model has strong contrast parameters and a small stratum thickness. Figures 6–8 display inversion results for the noise-added initial model, and show that NJI (Figures 6a, 7a, and 8a) produces stable results compared with LJI (Figures 6b, 7b, and 8b).

Figures 3–8 show that inversion methods based on exact Zoepritz solutions pick up the thin low-impedance layer in the true model. The inverted P- and S-wave velocities are closer to the true model values than are the inverted densities because density exhibits little sensitivity to amplitudes and the use of angle-limited AVA data may have affected its stability (Lines, 1998; Alemie and Sacchi, 2011; Du and Yan, 2013). However, for the model described in Table 1, larger incidence angles will cause critical reflectivity. A mean shift method, which is used to constrain the inversion procedure to improve the inversion accuracy, was applied to the NJI model results when the initial model was linear. As shown in Figure 9, the inversion constrained by the mean shift method is virtually identical to the true model.

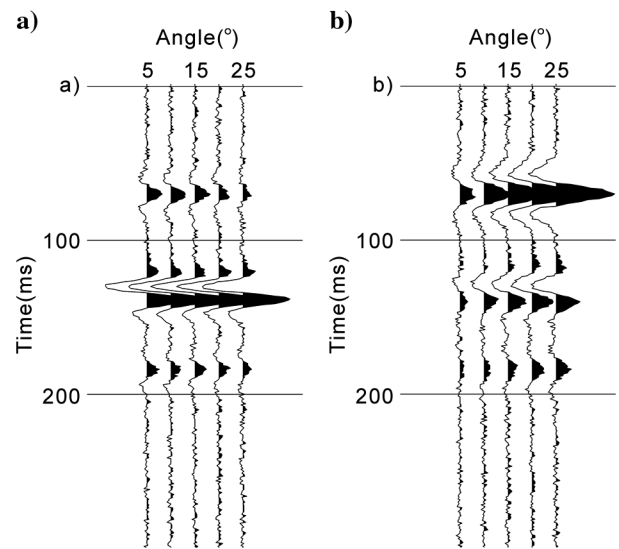


Figure 10. Synthetic (a) PP and (b) PS AVA records with a noise level of 16%.

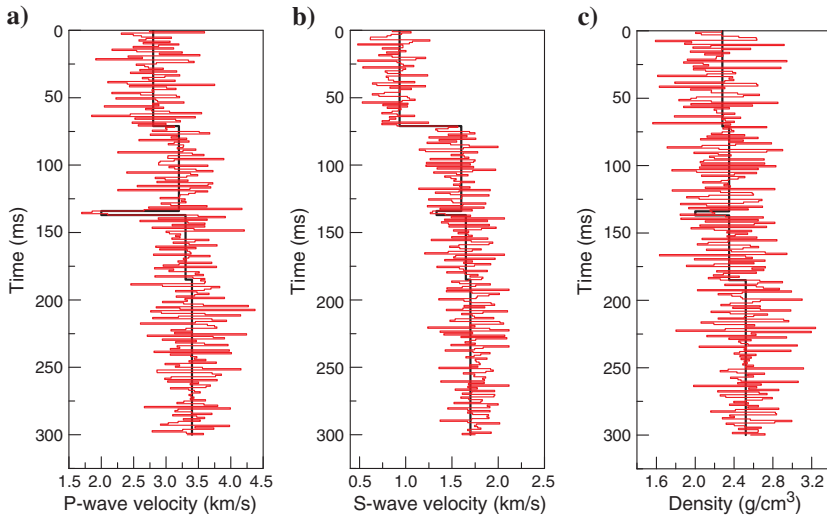


Figure 11. Inversion results by NJI method: (a) P-wave velocity, (b) S-wave velocity, and (c) density. The red curve is the NJI inversion result with 1% noise added to the synthetic PP and PS AVA records, and the black curve is the true model.

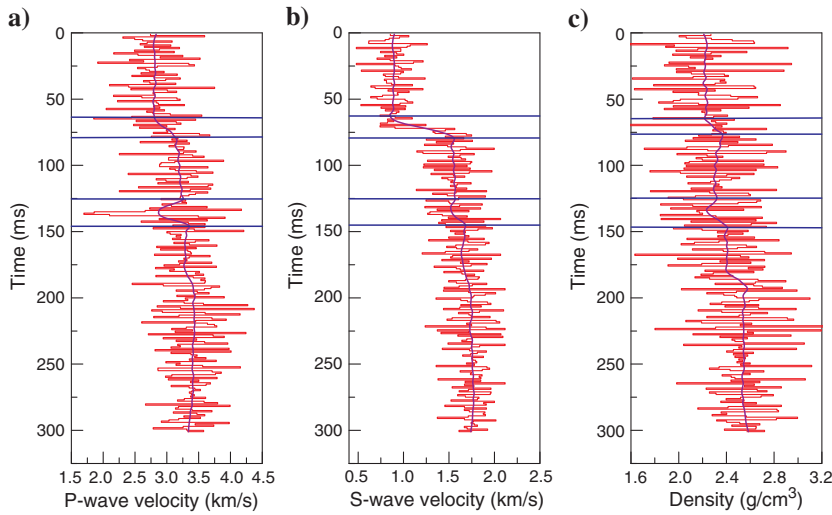


Figure 12. The trend lines calculated by the low-pass filtered NJI results: (a) P-wave velocity, (b) S-wave velocity, and (c) density. The red curve is the NJI result, the purple curve is the trend line, and the blue line marks the turning point in the trend line.

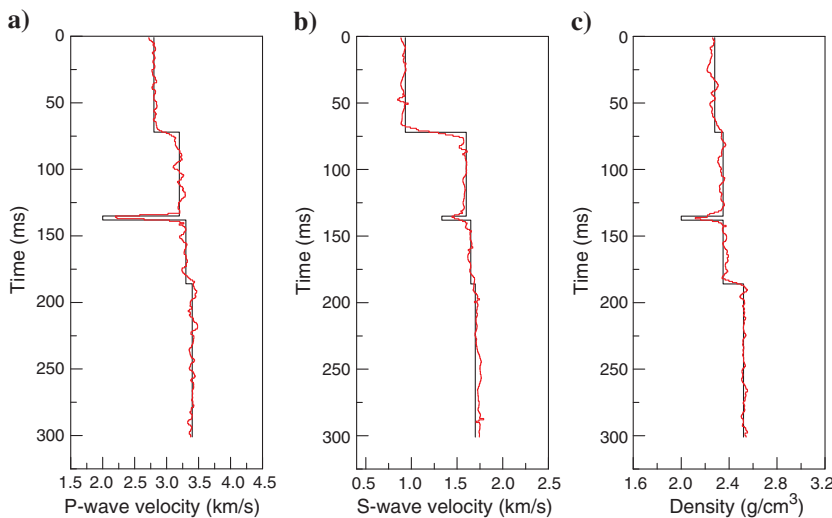


Figure 13. Inversion results by NJI method where the red curve represents the NJI inversion result shown in Figure 11 smoothed by piecewise smoothing algorithm, and the black curve is the true model.

Any acquired seismic record will contain a certain amount of noise, and inversion accuracy is highly dependent upon this noise level. To assess the sensitivity of our method to noise, we add random noise with different weights to the synthetic PP and PS seismograms separately. As shown in Figure 10, a noise level of 16% was generated randomly in the time domain, with noise values distributed normally around the synthetic signal.

Figure 11 shows the NJI results overlaid with the true values when 1% noise was added to the AVA records. The inversion result is close to the true model, including the thin layer with large elastic

contrasts, even though it is noisy. To suppress the noise for the inversion, we smoothed the inversion model values using a piecewise smoothing algorithm to obtain an improved inversion result. First, as shown in Figure 12, a low-pass filter is applied to get the trend line of the inversion results. Second, the turning points are distinguished from the trend line for dividing the trend line into several segments. Finally, the inversion result is smoothed in each segment. The smoothing results at the noise level of 1% are shown in Figure 13, and the results reveal the thin layer more effectively. The smoothing method also produces stable NJI results when a noise level of approximately 16% was added to the synthetic data (Figure 14).

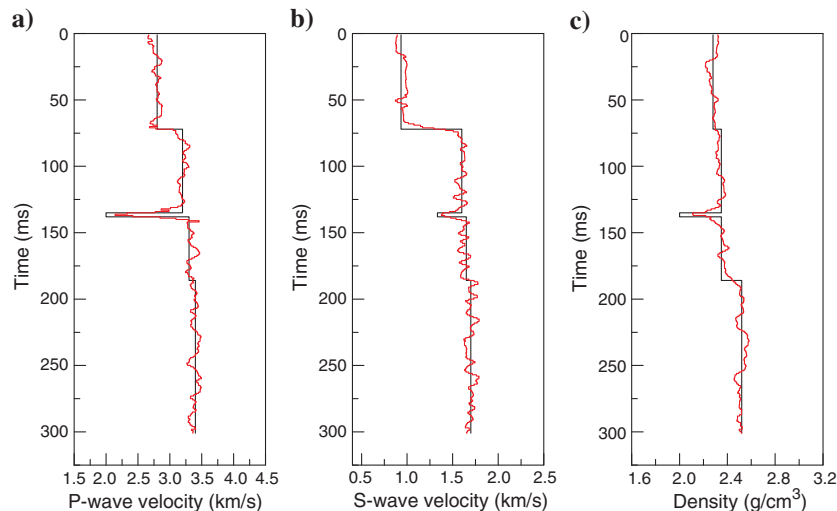


Figure 14. Inversion results by NJI method: (a) P-wave velocity, (b) S-wave velocity, and (c) density, where the red curve is smoothed using piecewise smoothing algorithm from the NJI inversion result with 16% noise added to the synthetic PP and PS AVA records, and the black curve is the true model.

### INVERSION OF FIELD MULTICOMPONENT DATA

Our inversion method has also been applied to a field multicomponent data. The inversion results are also compared with real well-log data. The field data are 2D with 1 ms sample rate and 118 common depth points (CDPs) in the Sichuan Basin, West China, and the CDP spacing is 10 m. The angle gather at the well location is shown in Figure 15. At the well location, P- and S-waves, as well as density logs were acquired and carefully processed. Before applying the NJI method, we carry out processing procedures, preserving the true amplitude of the seismic data. The first step is a static correction, which can flatten PP and PS events during the conversion of offset gather to incidence angle gather.

The second step is to calibrate PP and PS events reflected from each geologic interface in the PP traveltimes domain with the assistance

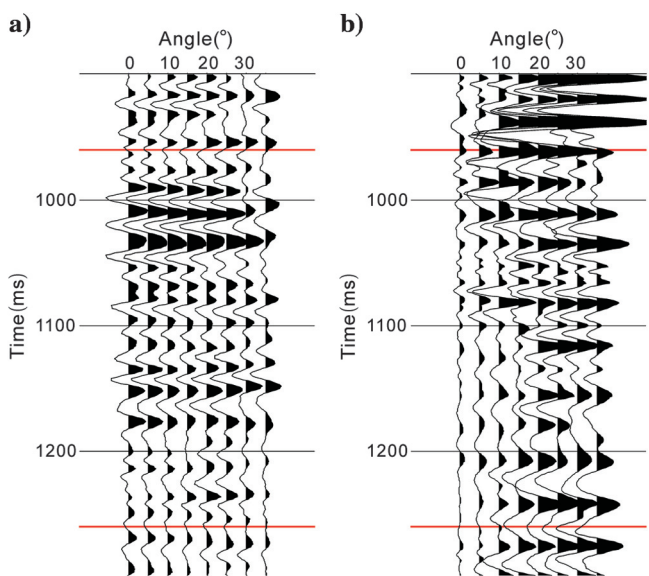


Figure 15. Time aligned field AVA data set. (a) Field PP AVA data set and (b) field PS AVA data set in the PP time domain. The NJI was performed for the time window 960–1260 ms, as indicated by the horizontal red lines.

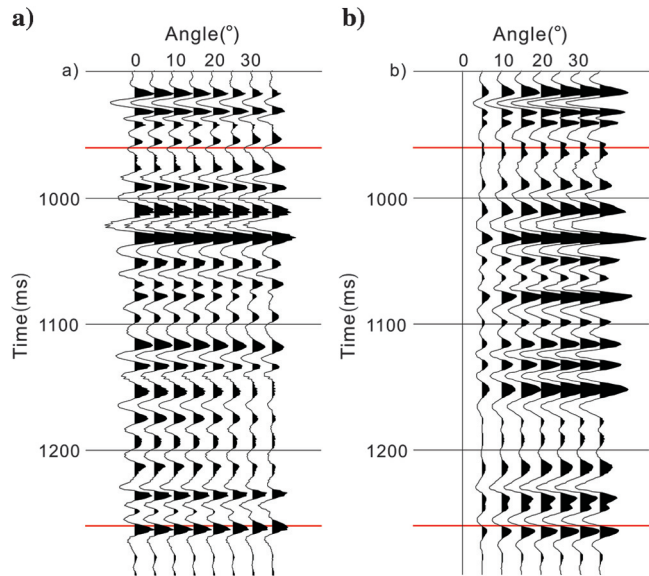


Figure 16. Time aligned synthetic AVA data set. (a) Synthetic PP AVA data set and (b) synthetic PS AVA data set in the PP time domain. The PP and PS AVA data sets are synthesized from the log data.

of synthetic seismograms calculated from well logs (Figure 16). During this procedure, PP and PS time-to-depth log conversions are calculated and used for PS data set compression. Compared with

Figure 16, it can be seen that the PP and PS seismograms in the PP traveltide domain shown in Figure 15 correlate well with synthetic seismograms after event correlation. Though the PS-field AVA data

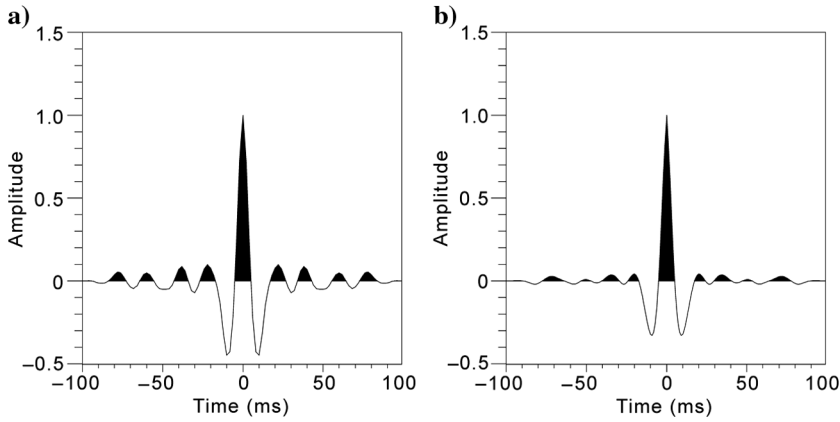


Figure 17. Wavelet extracted from time aligned data. (a) Wavelet of the PP AVA data set and (b) wavelet of the PS AVA data set, after compressing to the PP traveltide domain.

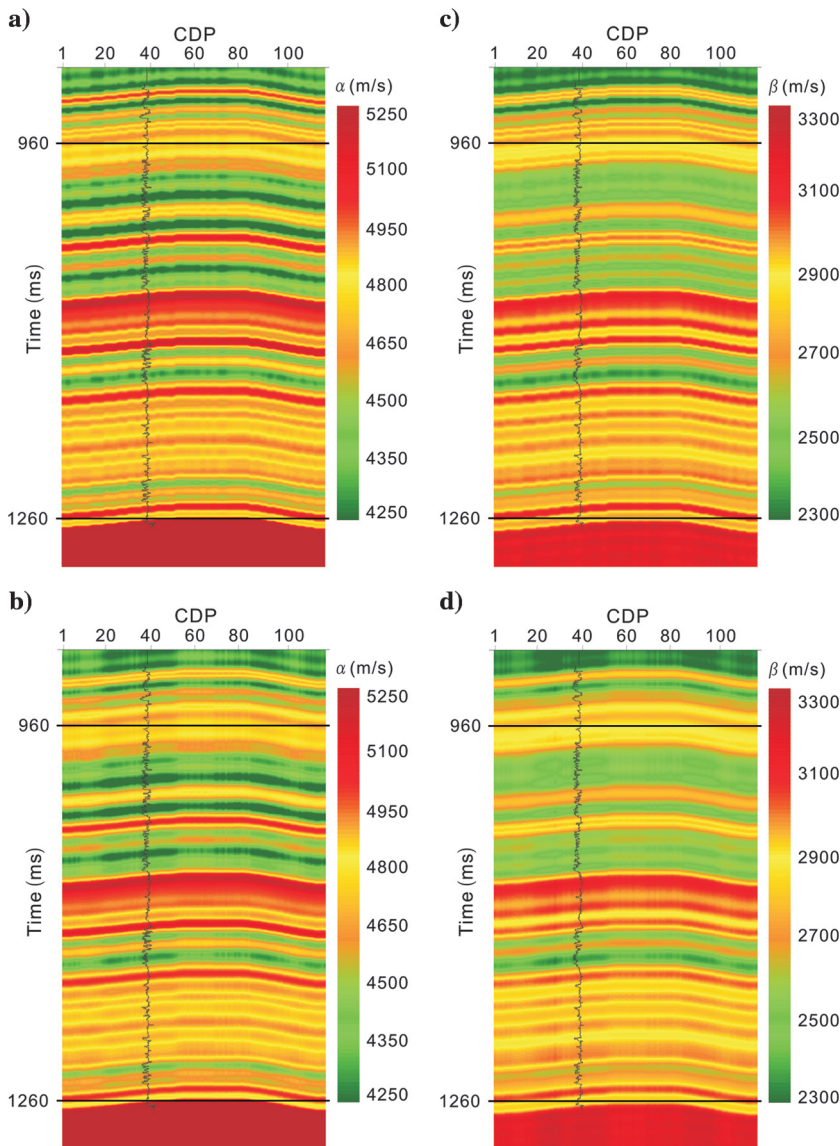


Figure 18. Inverted sections: (a) P-wave velocity by NJI method, (b) P-wave velocity by LJI method, (c) S-wave velocity by NJI method, and (d) S-wave velocity by LJI method. The black curve is the well log.

set is formed from the raw data with a worse signal-to-noise ratio, its correlation coefficient with the synthetic data set is up to 0.65 after careful processing. The correlation coefficient between the actual and synthetic PP AVA data sets is 0.76. So, we set the weight factor  $w$  in equation 5 to 0.5 because the two correlation coefficients are close.

The final step is to extract wavelets of PP and PS AVA data sets separately. We extract the statistical wavelets over the entire incidence angle range separately after event correlation. Figure 17 shows that both wavelets are zero phase and have similar main frequencies but differing side lobes.

The inverted sections are shown in Figures 18 and 19, where the green and red colors represent the shale and the sand contents of the layer, separately, which are calibrated by well logs. It shows that we can distinguish more thin layers from the sections inverted by the NJI method than by the LJI method. Compared with the other parameters, the velocity-ratio section (Figure 19c) inverted by NJI method shows obviously higher resolution. The near-well inversion results are extracted from the sections and shown in

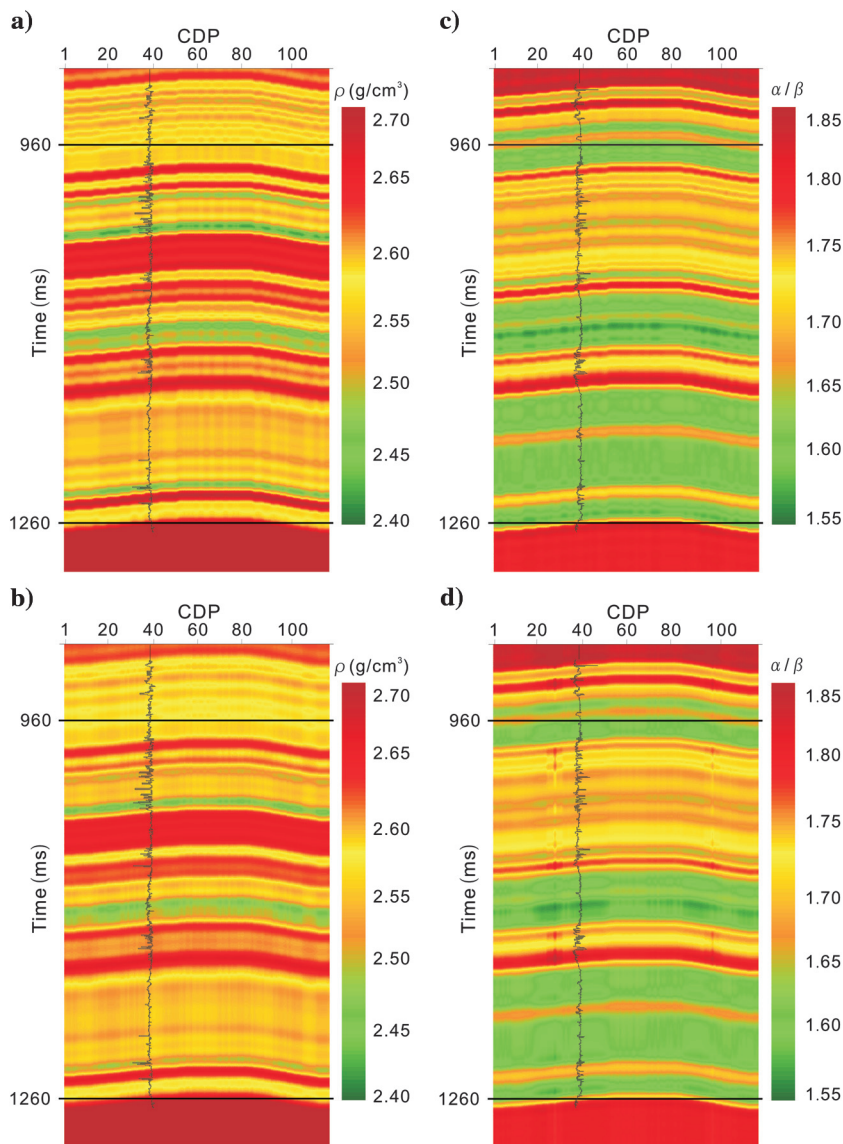
Figure 20. We can see that good calibration at the well position made the near-well inversion results closely match the well logs. Though the inversion results have lower frequency content than the well logs because of the limited frequency of the wavelet, NJI can produce a high-resolution result, which is beneficial to the recognition of thin layer.

## DISCUSSION

Our NJI inversion method requires careful data processing. Some true-amplitude processing techniques are mentioned in the above. Incidence angle is an important factor, which will affect the inversion result seriously. In cases of complicated structures, we can use a ray-tracing method to calculate the raypath at the target interface and derive the accurate incidence angle, which is out of the scope of this paper.

Noise attenuation is also quite important. Noise in the AVA data set will increase the uncertainty in the inversion result, but we can decrease the weight factor of the uncertain component to reduce the

Figure 19. Inverted sections: (a) density by NJI method, (b) density by LJI method, (c) P- to S-wave velocity ratios by NJI method, and (d) P- to S-wave velocity ratios by LJI method. The  $\alpha$  to  $\beta$  ratios are derived from the inverted P- and S-wave velocities. The black curve is the well log.



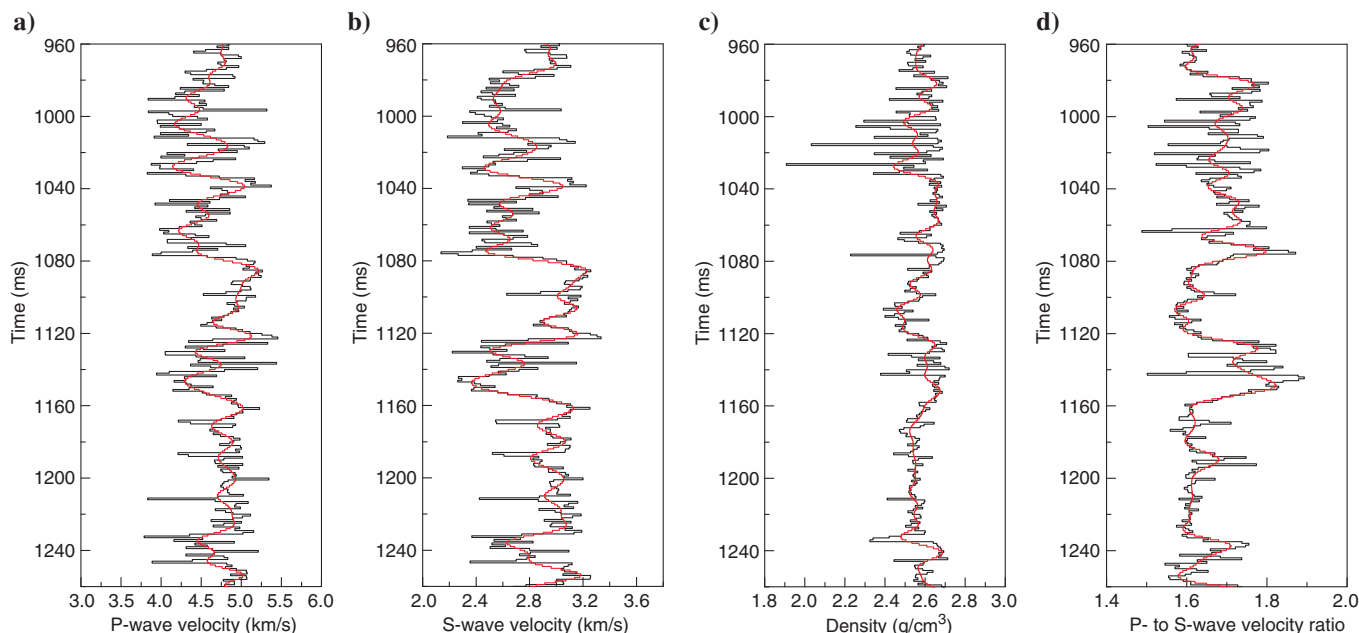


Figure 20. Near-well inversion results of NJI method (red curves) extracted from the sections: (a) P-wave velocity, (b) S-wave velocity, (c) density, and (d) P- to S-wave velocity ratios, where the black curves are well-log data.

noise effect. However, to distinguish thin layer information from the inversion result, we do not want the data to be filtered too hard before inversion.

Our inversion method does not consider anisotropy, so the negative effects of elastic parameter anisotropy on multicomponent seismic data must be eliminated. For vertical transverse isotropy (VTI) anisotropy, we can consider using a nonhyperbolic moveout correction technique to obtain large-angle data. Furthermore, in the case of horizontal transverse isotropy (HTI) anisotropy, phase error, induced by S-wave splitting, must be compensated in prestack processing. Many fast and slow S-wave separation methods can be used to compensate such phase error.

For thin layer models, it is hard to get the interface reflections only because the reflections from the top and bottom interfaces of the thin layer will interfere together and cannot be separated. Moreover, interbed multiples and converted waves are hard to suppress, also they will influence the amplitude and phase of the target reflection. Therefore, to pick up the thin layer from the inversion result of field data, it is necessary to deduce the reflection coefficient formula of the thin layer.

Event matching is crucial to joint PP and PS AVA inversion. The PS wavelet will change with time when compressed to PP time because of the time-variant compression ratio. Therefore, the PS wavelet should be extracted from the compressed data, and the time window chosen for inversion should be short enough to retain stability of the wavelet. It is necessary for us to explore a more effective method to improve event matching and PS-wave extraction in future work.

## CONCLUSIONS

We have developed a joint AVA inversion method (NJI) using the exact Zoeppritz equations for PP and PS seismic data, and we have

tested the model for synthetic and field seismic data. When dealing with high-contrast interfaces, inversion methods based on approximations to the Zoeppritz equations are insufficient, but our NJI method can achieve significantly better results.

The synthetic data example shows that it is possible to reveal a thin layer even with a linear initial model or with small amount of noise. The inverted elastic properties show a high level of random perturbation when a large amount of noise added to the synthetic data; however, the thin layer can still be revealed after a piecewise smoothing operation applied. Our NJI method is suitable for larger incidence angles, so velocity analysis and NMO corrections for large offset data must be applied before AVA gather formation; however, even in small incidence angle cases, the NJI method offers an advantage over approximation methods because it uses fewer theoretical assumptions. Also, the methodology requires noise suppression in AVA gathers, even though stable results can be achieved if the noise level is small.

For field data, our NJI method proved helpful in geologic layer interpretation, even though the PP- and PS-wavelets were narrow. We anticipate that our NJI method would be especially useful in predicting lithology and fluid properties in fields with thin and low-impedance layers.

## ACKNOWLEDGMENTS

We greatly appreciate the support of PetroChina Innovation Foundation (2011D-5006-0303), the Natural Science Foundation of China (41104084), and the Fundamental Research Funds for the Central Universities (2-9-2013-093). We are very grateful to Z. Li for sharing the field data. Thanks to T. Chen and an anonymous reviewer, whose comments and suggestions significantly improved the manuscript.

## REFERENCES

- Aki, K., and P. Richards, 1980, Quantitative seismology: W. H. Freeman & Co.
- Alemie, W., and M. D. Sacchi, 2011, High-resolution three-term AVO inversion by means of a Trivariate Cauchy probability distribution: *Geophysics*, **76**, no. 3, R43–R55, doi: [10.1190/1.3554627](https://doi.org/10.1190/1.3554627).
- Buland, A., and H. Omre, 2003, Bayesian linearized AVO inversion: *Geophysics*, **68**, 185–198, doi: [10.1190/1.1543206](https://doi.org/10.1190/1.1543206).
- Downton, J. E., 2005, Seismic parameter estimation from AVO inversion: Ph.D. thesis, University of Calgary.
- Downton, J. E., and L. R. Lines, 2004, Three term AVO waveform inversion: 74th Annual International Meeting, SEG, Expanded Abstracts, 215–218.
- Du, Q. Z., and H. Z. Yan, 2013, PP and PS joint AVO inversion and fluid prediction: *Journal of Applied Geophysics*, **90**, 110–118, doi: [10.1016/j.jappgeo.2013.01.005](https://doi.org/10.1016/j.jappgeo.2013.01.005).
- Fatti, J. L., G. C. Smith, P. J. Vail, P. J. Strauss, and P. R. Levitt, 1994, Detection of gas in sandstone reservoirs using AVO analysis: A 3-D seismic case history using the geostack technique: *Geophysics*, **59**, 1362–1376, doi: [10.1190/1.1443695](https://doi.org/10.1190/1.1443695).
- Jin, S., 1999, Characterizing reservoir by using jointly P- and S-wave AVO analysis: 69th Annual International Meeting, SEG, Expanded Abstracts, 687–690.
- Jin, S., G. Cambois, and C. Vuillermoz, 2000, Shear-wave velocity and density estimation from PS-wave AVO analysis: Application to an OBS data set from the North Sea: *Geophysics*, **65**, 1446–1454, doi: [10.1190/1.1444833](https://doi.org/10.1190/1.1444833).
- Jonathan, A. E., and M. Baan, 2011, How reliable is statistical wavelet estimation?: *Geophysics*, **76**, no. 4, V59–V68, doi: [10.1190/1.3587220](https://doi.org/10.1190/1.3587220).
- Kurt, H., 2007, Joint inversion of AVA data for elastic parameters by bootstrapping: *Computers & Geosciences*, **33**, 367–382, doi: [10.1016/j.cageo.2006.08.012](https://doi.org/10.1016/j.cageo.2006.08.012).
- Larsen, J. A., 1999, AVO inversion by simultaneous P-P and P-S inversion: M.S. thesis, University of Calgary.
- Levenberg, K., 1944, A method for the solution of certain non-linear problems in least squares: *Quarterly of Applied Mathematics*, **2**, 164–168.
- Lines, L. R., 1998, Density contrast is difficult to determine from AVO: CREWES, Research report 10.
- Lu, J., Y. Wang, and C. Yao, 2012, Separating P- and S-waves in an affine coordinate system: *Journal of Geophysics and Engineering*, **9**, 12–18, doi: [10.1088/1742-2132/9/1/002](https://doi.org/10.1088/1742-2132/9/1/002).
- Mahmoudian, F., 2006, Linear AVO inversion of multi-component surface seismic and VSP data: M.S. thesis, University of Calgary.
- Mahmoudian, F., and G. F. Margrave, 2004, Three parameter AVO inversion with PP and PS data using offset binning: 74th Annual International Meeting, SEG, Expanded Abstracts, 240–243.
- Marquardt, D. W., 1963, An algorithm for least-squares estimation of non-linear inequalities: *Journal of the Society for Industrial and Applied Mathematics*, **11**, 431–441, doi: [10.1137/0111030](https://doi.org/10.1137/0111030).
- Ostrander, W. J., 1982, Plane-wave reflection coefficients for gas sands at nonnormal angles of incidence: 52nd Annual International Meeting, SEG, Expanded Abstracts, 216–218.
- Ostrander, W. J., 1984, Plane-wave reflection coefficients for gas sands at non-normal angles of incidence: *Geophysics*, **49**, 1637–1648, doi: [10.1190/1.1441571](https://doi.org/10.1190/1.1441571).
- Roberts, G., D. Went, K. Hawkins, G. Williams, N. Kabir, T. Nash, and D. Whitcombe, 2002, A case study of long-offset acquisition, processing and interpretation over the Harding Field, North Sea: 64th Annual International Conference and Exhibition, EAGE, Extended Abstracts, 27–30.
- Shuey, R. T., 1985, A simplification of the Zoeppritz equations: *Geophysics*, **50**, 609–614, doi: [10.1190/1.1441936](https://doi.org/10.1190/1.1441936).
- Smith, G. C., and P. M. Gidlow, 1987, Weighted stacking for rock property estimation and detection of gas: *Geophysical Prospecting*, **35**, 993–1014, doi: [10.1111/j.1365-2478.1987.tb00856.x](https://doi.org/10.1111/j.1365-2478.1987.tb00856.x).
- Stewart, R. R., 1990, Joint P and P-SV inversion: CREWES, Research report 2.
- Sun, P. Y., X. L. Lu, Y. P. Li, Y. Y. Yue, and H. F. Chen, 2008, Elastic parameter AVO approximations and their applications: 78th Annual International Meeting, SEG, Expanded Abstracts, 523–527.
- Tigrek, S., E. C. Slob, M. W. P. Dillen, S. A. P. L. Cloetingh, and J. T. Fokkema, 2005, Linking dynamic elastic parameters to static state of stress: Toward an integrated approach to subsurface stress analysis: *Tectonophysics*, **397**, 167–179, doi: [10.1016/j.tecto.2004.10.008](https://doi.org/10.1016/j.tecto.2004.10.008).
- Ursenbach, C. P., and R. R. Stewart, 2008, Two-term AVO inversion: Equivalences and new methods: *Geophysics*, **73**, no. 6, C31–C38, doi: [10.1190/1.2978388](https://doi.org/10.1190/1.2978388).
- van der Baan, M., 2008, Time-varying wavelet estimation and deconvolution by kurtosis maximization: *Geophysics*, **73**, no. 2, V11–V18, doi: [10.1190/1.2831936](https://doi.org/10.1190/1.2831936).
- Veire, H. H., and M. Landrø, 2006, Simultaneous inversion of PP and PS seismic data: *Geophysics*, **71**, no. 3, R1–R10, doi: [10.1190/1.2194533](https://doi.org/10.1190/1.2194533).
- Wang, Y. M., X. P. Wang, X. J. Meng, and X. M. Niu, 2011, Pre-stack inversion of wide incident angle seismic data: 81st Annual International Meeting, SEG, Expanded Abstracts, 2507–2511.
- Xu, Y., and J. C. Bancroft, 1997, Joint AVO analysis of PP and PS seismic data: CREWES, Research report 9.
- Zhi, L. X., S. Q. Chen, and X. Y. Li, 2013, Joint AVO inversion of PP and PS waves using exact Zoeppritz equation: 83rd Annual International Meeting, SEG, Expanded Abstracts, 457–461.
- Zhu, X. F., and G. McMechan, 2012, AVO inversion using the Zoeppritz equation for PP reflections: 82nd Annual International Meeting, SEG, Expanded Abstracts, doi: [10.1190/segam2012-0160.1](https://doi.org/10.1190/segam2012-0160.1).